


Article

Data-Driven Operation of Flexible Distribution Networks with Charging Loads

Guorui Wang¹, Zhenghao Qian¹, Xinyao Feng¹, Haowen Ren², Wang Zhou², Jinhe Wang², Haoran Ji^{3,*}
and Peng Li³

¹ Guangdong Power Grid Company Limited, Guangzhou 510060, China; wangguorui@gd.csg.cn (G.W.); qianzhenghao@gd.csg.cn (Z.Q.); fengxinyao@xxzx.gd.csg.cn (X.F.)

² China Southern Power Grid Digital Platform Technology Company, Guangzhou 510663, China; renhw@csg.cn (H.R.); zhouwang@csg.cn (W.Z.); wangjh2@csg.cn (J.W.)

³ Key Laboratory of Smart Grid of Ministry of Education, Tianjin University, Tianjin 300072, China; lip@tju.edu.cn

* Correspondence: jihaoran@tju.edu.cn; Tel.: +86-155-2260-4232

Abstract: The high penetration of distributed generators (DGs) and the large-scale charging loads deteriorate the operational status of flexible distribution networks (FDNs). A soft open point (SOP) can deal with operational issues, such as voltage violations and the high electricity purchasing cost of charging stations. However, the absence of accurate parameters poses challenges to model-based methods. This paper proposes a data-driven operation method of FDNs with charging loads. First, a data-driven model-free adaptive predictive control (MFAPC) approach is proposed to fully involve charging loads in the control of FDN without accurate network parameters. Then, a multi-timescale coordination control model of an SOP with charging loads is established to satisfy the demand of charging loads and improve the control performance. The effectiveness of the proposed method is numerically demonstrated on the modified IEEE 33-node distribution network. The results indicate that the proposed method can effectively reduce the electricity purchasing cost of charging stations and improve the operational performance of FDNs.

Keywords: flexible distribution networks (FDNs); soft open point (SOP); data-driven operation; charging loads; multi-timescale coordination



Citation: Wang, G.; Qian, Z.; Feng, X.; Ren, H.; Zhou, W.; Wang, J.; Ji, H.; Li, P. Data-Driven Operation of Flexible Distribution Networks with Charging Loads. *Processes* **2023**, *11*, 1592. <https://doi.org/10.3390/pr11061592>

Academic Editors: Ziming Yan, Rui Wang, Chuan He, Tao Chen and Zhengmao Li

Received: 6 May 2023
Revised: 20 May 2023
Accepted: 20 May 2023
Published: 23 May 2023



Copyright: © 2023 by the authors. Licensee MDPI, Basel, Switzerland. This article is an open access article distributed under the terms and conditions of the Creative Commons Attribution (CC BY) license (<https://creativecommons.org/licenses/by/4.0/>).

1. Introduction

The high penetration of distributed generators (DGs) and increasing scale of charging loads exacerbate the uncertainty of distribution networks, causing power fluctuations and voltage violations [1,2]. Novel power electronic devices, represented by soft open points (SOPs), can tackle these issues and promote the development of flexible distribution networks (FDNs) [3]. An FDN is defined as a closed-loop operation distribution network, in which multiple feeders are interconnected by power electronic devices with the flexible control of power flows [4]. Remarkably, the SOP-based flexible interconnection technology realizes the accurate and fast power flow control of connected feeders, which significantly changes the operation of FDNs. Therefore, the overall flexibility and controllability of FDNs are significantly better than those of traditional distribution networks.

Considering the large-scale integration of charging loads, the participating potential of charging loads in the control of FDNs needs to be exploited. Ref. [5] proposed a mixed integer linear model of power supply recovery for FDNs based on the optimal operation strategy of an SOP and electrical vehicles (EVs). As more EVs participate in vehicle-to-grid service, the interaction between FDNs and EVs is becoming a key issue that affects network operation and user participation. Ref. [6] proposed a vehicle-pile resource allocation approach based on a two-stage categorical hierarchical scheduling framework to solve the vehicle-pile assignment problem in near real time. In [7], a multiyear hybrid planning method based on cost–benefit analysis was proposed for the implementation of excellent

EV charging strategies in FDNs. Ref. [8] proposed a coordinated day-ahead and real-time optimization model for FDNs with SOP and high penetration of EVs, where the day-ahead and real-time models were linearized. Ref. [9] established a random model to minimize operational cost, considering the uncertainty of DGs, load demand, plug-in hybrid EV demand and grid energy price. Considering the coupling of multiple devices, time-series coordination can be further implemented in the operation model of FDNs.

Furthermore, devices with time-series characteristics such as EVs are suggested to be scheduled in a longer time interval due to their physical mechanisms and lifetime issues. However, operation violations may occur within shorter time intervals due to fast fluctuations in FDNs. To address such unexpected issues, it is necessary to consider the coordination of various control devices on different timescales in FDNs. Ref. [10] proposed a two-stage voltage control strategy based on deep reinforcement learning to cope with the voltage violations caused by the uncertain behaviors of charging loads. Ref. [11] proposed a data center energy-saving method by optimizing IT equipment to realize large-scale and diverse uses of DGs. Ref. [12] established a multi-scheme multi-objective collaborative optimization model to effectively smooth voltage fluctuations. Based on the coordinated EV charging strategy, ref. [13] proposed a multi-stage optimal scheduling method to generate the day-ahead scheduling strategy. Ref. [14] dispatched surplus reactive power from charging loads and DGs for the optimized voltage support based on the average consensus theory and sensitivity analysis.

However, the traditional control methods depend on the detailed mathematical model and accurate physical parameters of FDNs. The control performance based on physical parameter modeling is limited by complex operation states, topology changes, and inaccurate physical parameters of FDNs. In addition, the increasing complexity and numerous components result in a heavy calculation burden, which is difficult to meet real-time requirements.

With the development of digitization, sufficient operational data support the application of data-driven control methods [15]. Ref. [16] developed a data-driven open-source simulation environment, ACN-Sim, which provided a modular and scalable architecture for EV charging. Ref. [17] established a data-driven distributed EV model with a voltage control function of microgrids to adjust the voltage and frequency of microgrids. Ref. [18] proposed a load forecasting model based on the long short-term memory network to optimize the operation of building energy supply systems integrated with EVs. Considering the uncertainty around the battery state of charge (SOC), ref. [19] proposed a coordinated scheduling strategy of EVs and thermostatically controlled loads to address the variability of charging loads in FDNs.

Model-free adaptive predictive control (MFAPC) is a promising data-driven method, which has shown great potential in the control of FDNs. Ref. [20] applied MFAPC to suppress the disturbance of variable pitch systems and ensure the stability of wind power generation. An event-triggered MFAPC method was proposed in [21] to address the external disturbance of permanent magnet synchronous motor systems. The predictive accuracy and robustness of MFAPC improve the control effect and overcome the uncertainty caused by the large-scale integration of DGs and EVs. However, uncoordinated control methods may be difficult to meet practical operational requirements of FDNs. It is essential to promote the data-driven multi-timescale coordination control method.

To address inaccurate parameters and diverse operational demands of FDNs, a framework of data-driven operation of FDNs with charging loads is proposed based on MFAPC. Considering the demand of charging loads and the rapid fluctuations of DGs, a multi-timescale coordination control model of an SOP with charging loads is proposed. The target is to reduce the electricity purchasing cost of charging stations while alleviating the voltage violations caused by DGs and charging loads. The main contributions of this paper are summarized as follows.

(1) A data-driven control framework of FDNs based on MFAPC is proposed to satisfy the time-series constraints of charging loads. By fully excavating the multi-source data, the

proposed framework can effectively cope with the inaccuracy of network parameters and improve the control effect of FDNs.

(2) Considering the charging behaviors of charging loads and the rapid regulation ability of an SOP, a multi-timescale coordination control model is established. The potential of charging loads is exploited to participate in the control of FDNs. The proposed control model can reduce the electricity purchasing cost of charging stations and alleviate the voltage violations of FDNs.

The remainder of this paper is organized as follows. Section 2 introduces the framework of the data-driven operation of FDNs with charging loads. Section 3 describes the data-driven control method based on MFAPC in detail. The case studies and analysis are presented in Section 4. Finally, the conclusions are drawn in Section 5.

2. Framework of Data-Driven Operation of FDNs with Charging Loads

The conventional model predictive control (MPC) method with a fixed optimization horizon has trouble coping with the uncertainty caused by the stochastic integration of charging loads in FDNs. Therefore, the MFAPC method is utilized to meet the operation demands of FDNs and charging loads.

Figure 1 shows the framework of data-driven operation of FDNs based on MFAPC. Considering the random arrival and departure of each charging load, the prediction horizon and control window are defined. In this paper, charging loads mainly refer to EVs. Due to the charging behaviors of EVs and their expected level of SOC, it is necessary to utilize the predictive control on the slow timescale. Moreover, to deal with the uncertainties and rapid fluctuations of DGs and charging loads, the real-time control ability of an SOP is utilized on the fast timescale. Based on measurement data, historical data, predictive data, and various equipment parameters, the data-driven multi-timescale coordination control model can be established and dynamically adjusted.

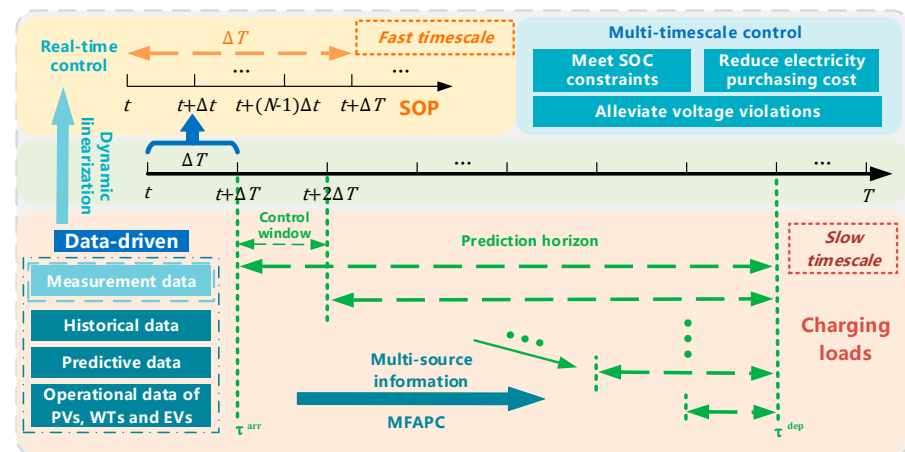


Figure 1. Framework of data-driven operation of FDNs based on MFAPC.

By utilizing the multi-timescale coordination control framework, the charging demands of EVs are satisfied, while the electricity purchasing cost of charging stations is reduced. Simultaneously, the rapid changes of time-varying parameters can be tracked by the data-driven dynamic linearization in the proposed framework, which can effectively respond to frequent changes in the operating state of FDNs.

3. Multi-Timescale Data-Driven Operation Based on MFAPC

3.1. Data-Driven Operation Model of FDNs with Charging Loads

Facing the challenge of inaccurate parameters and diverse operational demands of FDNs under complex operation environments, a data-driven control framework is proposed based on MFAPC to dynamically realize the adaptive predictive control in FDNs with charging loads. The essence of the data-driven predictive operation of devices with

time-series characteristics is to establish the relationship between control objectives and control strategies.

Specifically, considering the deviation from the reference of control objectives and the fluctuation penalty of control strategies, the objective function of the data-driven model based on MFAPC can be briefly established as shown in (1).

$$\mathcal{F}(\mathbf{X}_t) = \|\mathbf{Y}^{\text{ref}} - \hat{\mathbf{Y}}_{t+\Delta T}\|_2^2 + \lambda \|\mathbf{X}_t - \mathbf{X}_{t-\Delta T}\|_2^2 \quad (1)$$

where \mathbf{Y}^{ref} denotes the reference of the control objective. $\hat{\mathbf{Y}}_{t+\Delta T}$ denotes the predictive control objective at instant $t + \Delta T$. ΔT denotes the slow timescale. \mathbf{X}_t and $\mathbf{X}_{t-\Delta T}$ denote control strategies at instant t and $t - \Delta T$, respectively. $\lambda \|\mathbf{X}_t - \mathbf{X}_{t-\Delta T}\|_2^2$ is utilized to restrain the fluctuations of control strategy.

The predictive control objective is the sum of its initial value and variation.

$$\hat{\mathbf{Y}}_{t+\Delta T} = \mathbf{Y}_t^0 + \Delta \mathbf{Y}_{t+\Delta T} \quad (2)$$

where \mathbf{Y}_t^0 denotes the initial value of control objective at instant t , which can be obtained from historical data. $\Delta \mathbf{Y}_{t+\Delta T}$ denotes the variation of control objective at instant $t + \Delta T$.

Considering the regulation effect of multiple devices on the control objective, the variation of control objective can be divided into two parts corresponding to different timescales.

$$\Delta \mathbf{Y}_{t+\Delta T} = \Delta \mathbf{Y}_{t+\Delta T}^{\text{slow}} + \Delta \mathbf{Y}_{t+\Delta T}^{\text{fast}} \quad (3)$$

where $\Delta \mathbf{Y}_{t+\Delta T}^{\text{slow}}$ denotes the predictive variation of the control objective regulated on the slow timescale at instant $t + \Delta T$. Δt denotes the fast timescale. $\Delta \mathbf{Y}_{t+\Delta T}^{\text{fast}}$ denotes the extended variation of the control objective regulated on the fast timescale at instant $t + \Delta t$. Actually, $\Delta \mathbf{Y}_{t+\Delta T}^{\text{slow}}$ is regulated by devices with time-series characteristics such as distributed storage energy systems and EVs. $\Delta \mathbf{Y}_{t+\Delta T}^{\text{fast}}$ is regulated by controllable power electronic devices such as SOP and DG converters.

On the slow timescale, the dynamic estimation of the control objective is shown as follows.

$$\Delta \mathbf{Y}_{t+\Delta T}^{\text{slow}} = \Theta_t \Delta \hat{\mathbf{X}}_t^{\text{slow}} \quad (4)$$

$$\Delta \mathbf{Y}_{t+\Delta T}^{\text{slow}} = \left[\Delta \mathbf{Y}_{t+\Delta T}^{\text{slow} \text{ T}}, \Delta \mathbf{Y}_{t+2\Delta T}^{\text{slow} \text{ T}}, \dots, \Delta \mathbf{Y}_{t+N\Delta T}^{\text{slow} \text{ T}} \right]^{\text{T}} \quad (5)$$

$$\Theta_t = \text{diag}(\mathbf{S}_t, \mathbf{S}_{t+\Delta T}, \dots, \mathbf{S}_{t+(N-1)\Delta T}) \quad (6)$$

$$\Delta \hat{\mathbf{X}}_t^{\text{slow}} = \left[\Delta \mathbf{X}_t^{\text{slow} \text{ T}}, \Delta \mathbf{X}_{t+\Delta T}^{\text{slow} \text{ T}}, \dots, \Delta \mathbf{X}_{t+(N-1)\Delta T}^{\text{slow} \text{ T}} \right]^{\text{T}} \quad (7)$$

$$\Delta \mathbf{X}_t^{\text{slow}} = \mathbf{X}_t^{\text{slow}} - \mathbf{X}_{t-\Delta T}^{\text{slow}} \quad (8)$$

where $\Delta \mathbf{Y}_{t+\Delta T}^{\text{slow}}$, $\Delta \mathbf{Y}_{t+2\Delta T}^{\text{slow}}$ and $\Delta \mathbf{Y}_{t+N\Delta T}^{\text{slow}}$ denote control objectives regulated on the slow timescale at instant $t + \Delta T$, $t + 2\Delta T$, and $t + N\Delta T$, respectively. N denotes the number of remainder slow timescale from instant t to the end of the total control horizon. Θ_t denotes the predictive sensitivity block diagonal matrix on the slow timescale at instant t . \mathbf{S}_t , $\mathbf{S}_{t+\Delta T}$ and $\mathbf{S}_{t+(N-1)\Delta T}$ denote the slow-timescale sensitivity matrices at instances t , $t + \Delta T$, and $t + (N - 1)\Delta T$, respectively, which can be obtained from historical data. $\Delta \hat{\mathbf{X}}_t^{\text{slow}}$ denotes the predictive variation of control strategy on the slow timescale at instant t . $\Delta \mathbf{X}_t^{\text{slow}}$, $\Delta \mathbf{X}_{t+\Delta T}^{\text{slow}}$, and $\Delta \mathbf{X}_{t+(N-1)\Delta T}^{\text{slow}}$ denote the variations of control strategy on the slow timescale at instances t , $t + \Delta T$ and $t + (N - 1)\Delta T$, respectively.

The time-series constraint can be briefly expressed as (9).

$$\underline{\mathcal{C}}_{t,x} \leq \mathcal{G}_x(\mathbf{X}_t^{\text{slow}}, \mathbf{X}_{t+\Delta T}^{\text{slow}}, \dots, \Delta \mathbf{X}_{t+(N-1)\Delta T}^{\text{slow}}) \leq \bar{\mathcal{C}}_{t,x} \quad (9)$$

where ϑ_x denotes the undefined expression. $\underline{C}_{t,x}$ and $\overline{C}_{t,x}$ denote the lower and the upper bounds of the time-series constraint at instant t .

On the fast timescale, controllable power electronic devices without time-series constraints rapidly respond to the DG fluctuations so that there is no need to predict their strategy. The detailed extension of the variations of the control objective is expressed as follows.

$$\Delta \mathbf{Y}_{t+\Delta t}^{\text{fast}} = \left[\Delta \mathbf{Y}_{t+\Delta t}^{\text{fast} \text{ T}}, \mathbf{0}, \mathbf{0}, \dots, \mathbf{0} \right]^{\text{T}} \quad (10)$$

where $\Delta \mathbf{Y}_{t+\Delta t}^{\text{fast}}$ denotes the variation of the control objective regulated on the fast timescale at instant $t + \Delta t$. Zero vectors in $\Delta \mathbf{Y}_{t+\Delta t}^{\text{fast}}$ raise it to the same dimension as $\Delta \mathbf{Y}_{t+\Delta T}^{\text{slow}}$.

$$\Delta \mathbf{Y}_{t+\Delta t}^{\text{fast}} = \hat{\Phi}_t \Delta \mathbf{X}_t^{\text{fast}} \quad (11)$$

$$\Delta \mathbf{X}_t^{\text{fast}} = \mathbf{X}_t^{\text{fast}} - \mathbf{X}_{t-\Delta t}^{\text{fast}} \quad (12)$$

where $\hat{\Phi}_t$ denotes the estimation of the fast-timescale sensitivity matrix at instant t . $\Delta \mathbf{X}_t^{\text{fast}}$ denotes the variation of control strategy on the fast timescale at instant t . $\mathbf{X}_t^{\text{fast}}$ denotes the control strategy on the fast timescale at instant t .

The control strategy on the fast timescale can be directly solved by the gradient descent, considering the simple constraints of the controllable power electronic devices.

$$\mathbf{X}_t^{\text{fast}} = \mathbf{X}_{t-\Delta t}^{\text{fast}} + \frac{\rho \hat{\Phi}_t^{\text{T}} (\mathbf{Y}^{\text{ref}} - \mathbf{Y}_t^{\text{fast}})}{\lambda + \|\hat{\Phi}_t^{\text{T}}\|_{\text{F}}^2} \quad (13)$$

On the slow timescale, the control strategy of devices with time-series characteristics maintains a constant value while the control strategy is updated per fast timescale. $\mathbf{X}_t^{\text{slow}}$ maintains a constant value while $\mathbf{X}_t^{\text{fast}}$ is updated per Δt .

The fast-timescale sensitivity matrix can be estimated by the following parameter estimation function.

$$\min F(\Phi_t) = \|\Delta \mathbf{Y}_t - \Phi_t \Delta \mathbf{X}_t\|_2^2 + \mu \|\Phi_t - \hat{\Phi}_{t-\Delta t}\|_{\text{F}}^2 \quad (14)$$

where $\mu \|\Phi_t - \hat{\Phi}_{t-\Delta t}\|_{\text{F}}^2$ can reduce the fluctuations of parameter estimation.

Equations (13) and (14) can be solved by the gradient descent to obtain the estimation of the fast-timescale sensitivity matrix, which is shown in (15).

$$\hat{\Phi}_t = \hat{\Phi}_{t-\Delta t} + \frac{\eta \Delta \mathbf{X}_{t-\Delta t}^{\text{fast}} \left(\Delta \mathbf{Y}_t^{\text{fast}} - \hat{\Phi}_{t-\Delta t} \Delta \mathbf{X}_{t-\Delta t}^{\text{fast}} \right)}{\mu + \|\Delta \mathbf{X}_{t-\Delta t}^{\text{fast}}\|_2^2} \quad (15)$$

The data-driven multi-timescale coordination operation model of FDN can be summarized as:

$$\begin{aligned} \min F(\mathbf{X}_t) &= \|\mathbf{Y}^{\text{ref}} - \hat{\mathbf{Y}}_{t+\Delta T}\|_2^2 + \delta_1 \|\Delta \hat{\mathbf{X}}_t^{\text{slow}}\|_2^2 + \delta_2 \|\Delta \mathbf{X}_t^{\text{fast}}\|_2^2 \\ &\text{s.t. (2)-(4), (6)-(13), (15);} \end{aligned} \quad (16)$$

where δ_1 and δ_2 denote the weight factors.

3.2. Multi-Timescale Coordination Control Model

In this paper, the device with time-series characteristics refers to EVs, and the controllable power electronic device refers to an SOP. Considering the physical coupling of EVs and SOPs, the charging station is connected to the DC side of an SOP, which is shown in Figure 2.

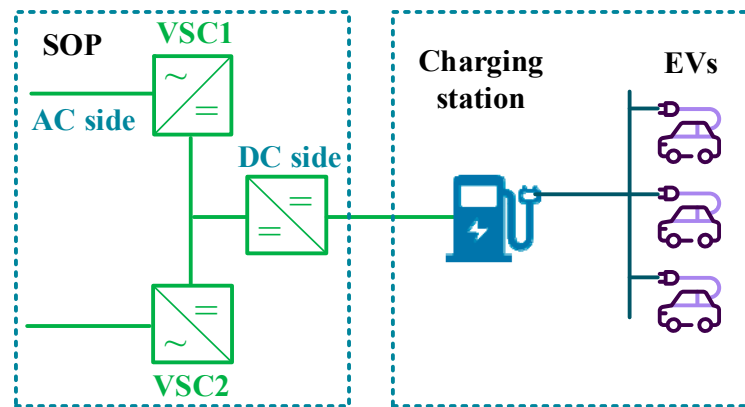


Figure 2. Diagram of the charging station connected to an SOP.

In the operation of FDNs with EVs, both the voltage quality on the network side and the electricity purchasing cost on the user side should be considered as control objectives. Therefore, to alleviate the voltage deviations of FDNs and reduce the electricity purchasing cost of the charging station, the optimization objective includes the electricity purchasing cost J_1 of the charging station and the voltage deviation cost J_2 . Measurements of nodal voltage and EV charging power are needed in the solution of the data-driven model. In addition, the penalty cost J_3 of control strategy is also considered to reduce the severe fluctuations of control devices.

$$\min J = J_1 + J_2 + J_3 \quad (17)$$

The electricity purchasing cost is shown as follows.

$$J_1 = \omega C_t^P P_t^{EV, \text{sum}} \quad (18)$$

where ω denotes the weight factor. C_t^P denotes the price at instant t . $P_t^{EV, \text{sum}}$ denotes the sum of EV charging power at instant t .

The voltage deviation cost at instant t is shown as follows.

$$J_2 = C_t^U (\mathbf{u}^{\text{ref}} - \hat{\mathbf{u}}_{t+\Delta T})^T (\mathbf{u}^{\text{ref}} - \hat{\mathbf{u}}_{t+\Delta T}) \quad (19)$$

where C_t^U denotes the penalty factor of voltage deviation at instant t . \mathbf{u}^{ref} denotes the voltage reference. $\hat{\mathbf{u}}_{t+\Delta T}$ denotes the predictive voltage at instant $t + \Delta T$.

The penalty cost of the control strategy can alleviate severe actions of the SOP and the charging station, which can be expressed as:

$$J_3 = \lambda_1 \Delta \hat{P}_t^{EV, \text{sum}^T} \Delta \hat{P}_t^{EV, \text{sum}} + \lambda_2 \Delta \mathbf{X}_t^{\text{SOP}^T} \Delta \mathbf{X}_t^{\text{SOP}} \quad (20)$$

where $\Delta \hat{P}_t^{EV, \text{sum}}$ denotes the predictive variation of the sum of the EV charging power at instant t . $\Delta \mathbf{X}_t^{\text{SOP}}$ denotes the variation of the control strategy of the SOP at instant t . λ_1 and λ_2 denote the weight factors.

Considering the controllable ability of SOPs and EVs, the voltage is regulated by the above devices. Thus, the predictive voltage variation should be divided into two parts, which are corresponding to the two kinds of devices. As for the details of voltage regulation, $\hat{\mathbf{u}}_{t+\Delta T}$ in objective function J_2 is shown as follows.

$$\hat{\mathbf{u}}_{t+\Delta T} = \mathbf{u}_t^0 + \Delta \mathbf{u}_{t+\Delta T} \quad (21)$$

$$\Delta \mathbf{u}_{t+\Delta T} = \Delta \mathbf{u}_{t+\Delta T}^{\text{EV}} + \Delta \mathbf{u}_{t+\Delta T}^{\text{SOP}} \quad (22)$$

where \mathbf{U}_t^0 denotes the predictive initial voltage at instant t , which can be obtained from historical data. $\Delta\mathbf{U}_{t+\Delta T}$ denotes the predictive voltage variation at instant $t + \Delta T$. $\Delta\mathbf{U}_{t+\Delta T}^{\text{EV}}$ denotes the predictive variation of voltage regulated by EVs at instant $t + \Delta T$. $\Delta\mathbf{U}_{t+\Delta T}^{\text{SOP}}$ denotes the extended variation of voltage regulated by the SOP at instant $t + \Delta T$.

On the slow timescale, $\Delta\mathbf{U}_{t+\Delta T}^{\text{EV}}$ is constant while $\Delta\mathbf{U}_{t+\Delta T}^{\text{SOP}}$ continuously updates per Δt . The predictive voltage regulated by EVs is shown as follows.

$$\Delta\mathbf{U}_{t+\Delta T}^{\text{EV}} = \Theta_t^{\text{EV}} \Delta\hat{\mathbf{P}}_t^{\text{EV,sum}} \quad (23)$$

$$\Theta_t^{\text{EV}} = \text{diag}(\mathbf{S}_t^{\text{EV}}, \mathbf{S}_{t+\Delta T}^{\text{EV}}, \dots, \mathbf{S}_{t+(N-1)\Delta T}^{\text{EV}}) \quad (24)$$

$$\Delta\hat{\mathbf{P}}_t^{\text{EV,sum}} = \left[\Delta P_t^{\text{EV,sum}}, \Delta P_{t+\Delta T}^{\text{EV,sum}}, \dots, \Delta P_{t+(N-1)\Delta T}^{\text{EV,sum}} \right]^T \quad (25)$$

$$\Delta P_t^{\text{EV,sum}} = P_t^{\text{EV,sum}} - P_{t-\Delta T}^{\text{EV,sum}} \quad (26)$$

where Θ_t^{EV} denotes the predictive sensitivity block diagonal matrix at instant t . \mathbf{S}_t^{EV} , $\mathbf{S}_{t+\Delta T}^{\text{EV}}$ and $\mathbf{S}_{t+(N-1)\Delta T}^{\text{EV}}$ denote the sensitivity matrices at instant t , $t + \Delta T$ and $t + (N - 1)\Delta T$, which can be obtained from historical data.

The sensitivity in (24) denotes the power-to-voltage sensitivity, where the voltage is regulated by EVs. The calculation of \mathbf{S}_t^{EV} can be shown as follows.

$$\mathbf{S}_t^{\text{EV}} = \frac{\sum_{\beta \in \text{B}} \frac{\partial \mathbf{u}_t^{\text{EV},\beta}}{\partial P_t^{\text{EV},\beta}}}{N_{\text{B}}} \quad (27)$$

where $\mathbf{u}_t^{\text{EV},\beta}$ denotes the voltage regulated by EVs in typical scheme β at instant t . $P_t^{\text{EV},\beta}$ denotes the EV charging power in typical scheme β at instant t . B denotes the set of typical schemes. N_{B} denotes the number of schemes in B.

In this paper, EVs are divided into two types according to the controllability of charge status. The charging power of type I EVs is constant. This type of EV can be charged as soon as it arrives at the charging station until the SOC reaches the expectation. The charging power of type II EVs is controllable, which can participate in the regulation of FDNs and respond to price guidance.

$$P_t^{\text{EV,sum}} = \sum_{n \in \Omega_{\text{I}}} P_{t,n}^{\text{I,C}} + \sum_{m \in \Omega_{\text{II}}} P_{t,m}^{\text{II,C}} \quad (28)$$

where $\Delta P_t^{\text{EV,sum}}$, $\Delta P_{t+\Delta T}^{\text{EV,sum}}$ and $\Delta P_{t+(N-1)\Delta T}^{\text{EV,sum}}$ denote variations of the sum of EV charging power at instant t , $t + \Delta T$ and $t + (N - 1)\Delta T$, respectively. $P_t^{\text{EV,sum}}$ and $P_{t-\Delta T}^{\text{EV,sum}}$ denote summaries of the EV charging power at instant t and $t + \Delta T$, respectively. Ω_{I} and Ω_{II} denote sets of EVs of type I and II, respectively. $P_{t,n}^{\text{I,C}}$ denotes the charging power of the n -th EV of type I at instant t . $P_{t,m}^{\text{II,C}}$ denotes the charging power of the m -th EV of type II at instant t .

The charging behaviors should be considered in the process of scheduling charging loads. EV behaviors can be approximated by the following probability density function (Zhu et al., 2018 [13]).

$$f(\tau_{\text{arr}}) = \begin{cases} \frac{1}{\sqrt{2\pi}\sigma_{\text{arr}}} \exp\left(-\frac{(\tau_{\text{arr}} - (\mu_{\text{arr}} - 24))^2}{2(\sigma_{\text{a}})^2}\right), & 0 < \tau_{\text{arr}} < \mu_{\text{arr}} - 12 \\ \frac{1}{\sqrt{2\pi}\sigma_{\text{arr}}} \exp\left(-\frac{(\tau_{\text{arr}} - \mu_{\text{arr}})^2}{2(\sigma_{\text{arr}})^2}\right), & \mu_{\text{arr}} - 12 < \tau_{\text{arr}} < 24 \end{cases} \quad (29)$$

$$f(\tau_{\text{dep}}) = \begin{cases} \frac{1}{\sqrt{2\pi}\sigma_{\text{dep}}} \exp\left(-\frac{(\tau_{\text{dep}} - \mu_{\text{dep}})^2}{2(\sigma_{\text{dep}})^2}\right), & 0 < \tau_{\text{dep}} < \mu_{\text{dep}} + 12 \\ \frac{1}{\sqrt{2\pi}\sigma_{\text{dep}}} \exp\left(-\frac{(\tau_{\text{dep}} - (\mu_{\text{dep}} + 24))^2}{2(\sigma_{\text{dep}})^2}\right), & \mu_{\text{dep}} + 12 < \tau_{\text{dep}} < 24 \end{cases} \quad (30)$$

where τ_{arr} and τ_{dep} denote the time when EVs arrive at and depart from the charging station. μ_{arr} and μ_{dep} are the mean values. σ_{arr} and σ_{dep} are the standard deviations.

The initial SOC when EVs arrive at the charging station can be modeled using a normal probability function.

$$f(s_{\text{arr}}) = \frac{1}{\sqrt{2\pi}\sigma_{\text{SOC}}} \exp\left(-\frac{(s_{\text{arr}} - \mu_{\text{SOC}})^2}{2(\sigma_{\text{SOC}})^2}\right) \quad (31)$$

where s_{arr} denotes the initial SOC when EVs arrive at the charging station. μ_{SOC} denotes the mean values. σ_{SOC} denotes the standard deviations.

The following relevant parameters of EVs obey the above distributions. The charging constraints of EVs of type I are shown as follows.

$$\tau_n^{\text{I,end}} = (s_n^{\text{I,E}} - s_n^{\text{I,arr}}) E_n^{\text{I,C}} / P_{t,n}^{\text{I,C}} + \tau_n^{\text{I,arr}} \quad (32)$$

$$\begin{cases} P_{t,n}^{\text{I,C}} = \bar{P}^{\text{EV}}, & \tau_n^{\text{I,arr}} \leq t < \tau_n^{\text{I,end}} \\ P_{t,n}^{\text{I,C}} = 0, & \tau_n^{\text{I,end}} \leq t \end{cases} \quad (33)$$

$$s_{t,n}^{\text{I}} = \begin{cases} s_n^{\text{I,arr}} & , & t = \tau_n^{\text{I,arr}} \\ s_{t-\Delta T,n}^{\text{I}} + P_{t,n}^{\text{I,C}} \Delta T / E_n^{\text{I,C}} & , & \tau_n^{\text{I,arr}} < t < \tau_n^{\text{I,dep}} \\ s_n^{\text{I,E}} & , & t = \tau_n^{\text{I,dep}} \end{cases} \quad (34)$$

where $\tau_n^{\text{I,end}}$ denotes the time when the n -th EV of type I finishes charging. $\tau_n^{\text{I,arr}}$ denotes the time when the n -th EV of type I arrives at the charging station. $s_{t,n}^{\text{I}}$ and $s_{t-\Delta T,n}^{\text{I}}$ denote the SOC of the n -th EV of type I at instant t and $t - \Delta T$, respectively. $s_n^{\text{I,E}}$ denotes the expected SOC of the n -th EV of type I. $s_n^{\text{I,arr}}$ denotes the initial SOC when the n -th EV of type I arrives at the charging station. $E_n^{\text{I,C}}$ denotes the capacity of the n -th EV of type I. \bar{P}^{EV} denotes the upper bound of the charging power. $\tau_n^{\text{I,dep}}$ denotes the time when the n -th EV of type I departs from the charging station.

The charging constraints of EVs of type II are shown as follows.

$$\begin{cases} 0 \leq P_{t,m}^{\text{II,C}} \leq \bar{P}^{\text{EV}}, & \tau_m^{\text{II,arr}} \leq t < \tau_m^{\text{II,dep}} \\ P_{t,m}^{\text{II,C}} = 0, & \tau_m^{\text{II,dep}} \leq t \end{cases} \quad (35)$$

$$s_{t,m}^{\text{II}} = \begin{cases} s_m^{\text{II,arr}} & , & t = \tau_m^{\text{II,arr}} \\ s_{t-\Delta T,m}^{\text{II}} + P_{t,m}^{\text{II,C}} \Delta T / E_m^{\text{II,C}} & , & \tau_m^{\text{II,arr}} < t < \tau_m^{\text{II,dep}} \end{cases} \quad (36)$$

where $\tau_m^{\text{II,arr}}$ denotes the time when the m -th EV of type II arrives at the charging station. $\tau_m^{\text{II,dep}}$ denotes the time when the m -th EV of type II departs from the charging station. $E_m^{\text{II,C}}$ denotes the capacity of the m -th EV of type II. $s_{t,m}^{\text{II}}$ and $s_{t-\Delta T,m}^{\text{II}}$ denote the SOC of the n -th EV of type II at instant t and $t - \Delta T$, respectively.

The SOC of EVs should reach the expectation when EVs depart from the charging station. In the solution of the control strategy at instant t , the charging power of EVs from $t + \Delta T$ to $t + (N - 1)\Delta T$ should be predicted. The sum of charging power from $t + \Delta T$ to

$t + (N - 1)\Delta T$ should ensure that the SOC of EVs reaches the expectation. The time-series constraint of EVs is shown as follows:

$$s_m^{\text{II,E}} \leq s_{t,m}^{\text{II}} + \frac{\Delta T}{E_m^{\text{II,C}}} \sum_{\tau=t+\Delta T}^{t+(N-1)\Delta T} P_{\tau,m}^{\text{II,C}} < \bar{s}_m^{\text{II}} \quad (37)$$

where $s_m^{\text{II,E}}$ denotes the expected SOC of the m -th EV of type II. $s_m^{\text{II,arr}}$ denotes the initial SOC when the m -th EV of type II arrives at the charging station. \bar{s}_m^{II} denotes the upper bound of SOC of the m -th EV of type II.

On the fast timescale, there is no need to predict the strategy of the SOP and the voltage regulated by the SOP so that zero vectors are utilized to expand the dimension of $\Delta \mathbf{u}_{t+\Delta t}^{\text{SOP}}$ according to (10).

$$\Delta \mathbf{u}_{t+\Delta t}^{\text{SOP}} = \left[\Delta \mathbf{u}_{t+\Delta t}^{\text{SOP,T}}, \mathbf{0}, \mathbf{0}, \dots, \mathbf{0} \right]^T \quad (38)$$

$$\Delta \mathbf{u}_{t+\Delta t}^{\text{SOP}} = \hat{\phi}_t^{\text{SOP}} \Delta \mathbf{x}_t^{\text{SOP}} \quad (39)$$

$$\Delta \mathbf{x}_t^{\text{SOP}} = \mathbf{x}_t^{\text{SOP}} - \mathbf{x}_{t-\Delta t}^{\text{SOP}} \quad (40)$$

$$\mathbf{x}_t^{\text{SOP}} = \left[P_{t,a}^{\text{SOP}}, P_{t,b}^{\text{SOP}}, Q_{t,a}^{\text{SOP}}, Q_{t,b}^{\text{SOP}} \right]^T \quad (41)$$

where $\Delta \mathbf{u}_{t+\Delta t}^{\text{SOP}}$ denotes the voltage variation regulated by the SOP at instant $t + \Delta t$. $\mathbf{0}$ denotes a zero vector. $\hat{\phi}_t^{\text{SOP}}$ denotes the sensitivity matrix of the SOP at instant t . $\mathbf{x}_t^{\text{SOP}}$ and $\mathbf{x}_{t-\Delta t}^{\text{SOP}}$ denotes control strategies of the SOP at instant t and $t - \Delta t$, respectively. a and b denote the two terminals of the SOP. $P_{t,a}^{\text{SOP}}$ and $P_{t,b}^{\text{SOP}}$ denote the active power transmission of two terminals of SOP at instant t . $Q_{t,a}^{\text{SOP}}$ and $Q_{t,b}^{\text{SOP}}$ denote the reactive power compensation of two terminals of the SOP at instant t .

The iterations of $\mathbf{x}_t^{\text{SOP}}$ and $\hat{\phi}_t^{\text{SOP}}$ are shown as follows according to (13) and (15).

$$\mathbf{x}_t^{\text{SOP}} = \mathbf{x}_{t-\Delta t}^{\text{SOP}} + \frac{\rho \hat{\phi}_t^{\text{SOP,T}} \left(\mathbf{u}_{t+\Delta t}^{\text{ref}} - \mathbf{u}_t^{\text{SOP}} \right)}{\lambda + \|\hat{\phi}_t^{\text{SOP,T}}\|_{\text{F}}^2} \quad (42)$$

$$\hat{\phi}_t^{\text{SOP}} = \hat{\phi}_{t-\Delta t}^{\text{SOP}} + \frac{\eta \Delta \mathbf{x}_{t-\Delta t}^{\text{SOP}} \left(\Delta \mathbf{u}_t^{\text{SOP}} - \hat{\phi}_{t-\Delta t}^{\text{SOP}} \Delta \mathbf{x}_{t-\Delta t}^{\text{SOP}} \right)}{\mu + \|\Delta \mathbf{x}_{t-\Delta t}^{\text{SOP}}\|_2^2} \quad (43)$$

In this paper, the charging station is connected to the DC side of an SOP. Thus, the following active/reactive power constraints should be satisfied.

$$\bar{P}^{\text{SOP}} \leq P_{t,a}^{\text{SOP}} \leq \underline{P}^{\text{SOP}} \quad (44)$$

$$\bar{P}^{\text{SOP}} \leq P_{t,b}^{\text{SOP}} \leq \underline{P}^{\text{SOP}} \quad (45)$$

$$\bar{Q}^{\text{SOP}} \leq Q_{t,a}^{\text{SOP}} \leq \underline{Q}^{\text{SOP}} \quad (46)$$

$$\bar{Q}^{\text{SOP}} \leq Q_{t,b}^{\text{SOP}} \leq \underline{Q}^{\text{SOP}} \quad (47)$$

$$\left(P_{t,a}^{\text{SOP}} \right)^2 + \left(Q_{t,a}^{\text{SOP}} \right)^2 \leq \left(C^{\text{SOP}} \right)^2 \quad (48)$$

$$\left(P_{t,b}^{\text{SOP}} \right)^2 + \left(Q_{t,b}^{\text{SOP}} \right)^2 \leq \left(C^{\text{SOP}} \right)^2 \quad (49)$$

$$P_{t,a}^{\text{SOP}} = P_t^{\text{EV,sum}} + P_{t,b}^{\text{SOP}} \quad (50)$$

where \bar{P}^{SOP} and $\underline{P}^{\text{SOP}}$ denote the upper and lower bounds of active power transmission through the SOP. \bar{Q}^{SOP} and $\underline{Q}^{\text{SOP}}$ denote the upper and lower bounds of the reactive power output of the SOP. C^{SOP} denotes the capacity of the SOP.

The data-driven multi-timescale coordination control model based on MFAPC can be summarized as:

$$\begin{aligned} \min J &= J_1 + J_2 + J_3 \\ \text{s.t.} & \text{ (21)–(28), (32)–(50);} \end{aligned} \quad (51)$$

Thus, based on the real-time measurement, the data-driven model can improve the control effect of FDNs without accurate physical parameters and reduce the electricity purchasing cost of charging stations.

3.3. Solution Methodology

The solution of the proposed method is shown in Figure 3. The detailed steps are shown as follows.

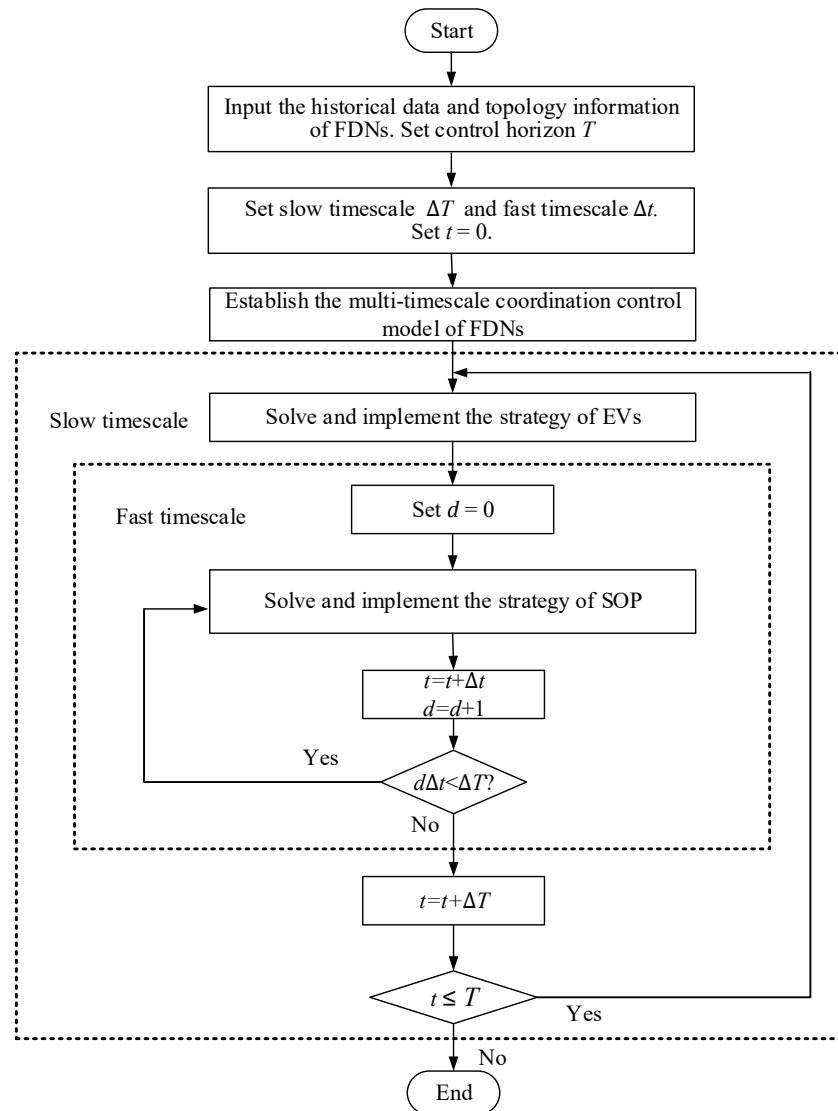


Figure 3. Flowchart of data-driven control of FDNs with EVs integration.

Step (1): Input the historical data and topology information of FDNs. Set control horizon T and multi-timescale parameters ΔT and Δt . Set $t = 0$.

Step (2): Utilize multi-source data to establish the multi-timescale coordination control model of FDNs. Solve and implement the strategy of EVs. Set $d = 0$.

Step (3): Solve and implement the strategy of the SOP. Set $t = t + \Delta t$, $d = d + 1$.

Step (4): If $\Delta t * d < \Delta T$, repeat Step (3). If $d\Delta t = \Delta T$, $t = t + \Delta T$.

Step (5): If $t \leq T$, repeat Step (2) to Step (4). Continuously update the model until $t = T$.

4. Case Studies and Analysis

The proposed data-driven operation control of FDN with charging loads is verified on the modified IEEE 33-node distribution network, whose topology and nodal number are the same as the standard IEEE 33-node distribution network. Its modification denotes the integration of DGs, SOPs, a charging station and EVs. The proposed method is implemented in MATLAB R2019a. The numerical experiments are carried out on a computer with Intel(R) Core(TM) i7-11700 @ 2.50 GHz and 16 GB of RAM.

4.1. Parameters

The topology of the modified IEEE 33-node distribution network is shown in Figure 4. The digital (1–33) in Figure 4 denotes the nodal number of the network, which is the same as the standard IEEE 33-node distribution network. The modified IEEE 33-node distribution network includes a substation and 32 branches, of which the rated voltage level is 12.66 kV. The total active power and reactive power demands are 3715.0 kW and 2300.0 kVar, respectively. Considering the high penetration of DGs, three photovoltaics (PVs) are installed at Nodes 7, 13, and 27, whose capacities are 500 kW_p, 300 kW_p, and 400 kW_p, respectively. Five wind turbines (WTs) are installed at Nodes 10, 16, 17, 30, and 33, whose capacities are 300 kVA, 200 kVA, 200 kVA, 200 kVA, and 300 kVA, respectively. An SOP with the capacity of 1400 kVA is installed between Nodes 18 and 33. Figure 5 shows the curves of DGs and loads.

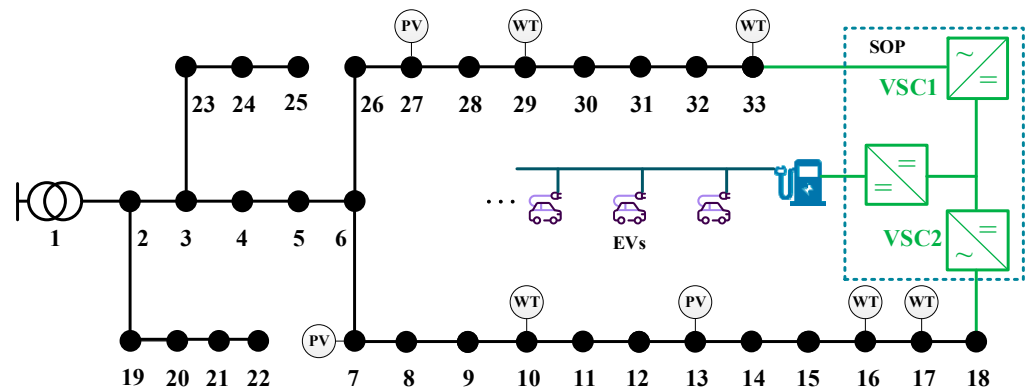


Figure 4. Structure of the modified IEEE 33-node distribution network.

The slow timescale ΔT is set as 1 h. The fast timescale Δt is set as 5 min. There are 100 EVs arriving at the charging station in the total control horizon. The factors μ , ρ , η and λ are set as 1. The factor ω is set as 100. C_t^U is set as 1.0 CNY/V². λ_1 and λ_2 are set as 1.0 CNY/(kW)² and 1 CNY/(kVA)², respectively. The number of EVs of type I is 25 and the number of EVs of type II is 75. The capacity of each EV is 100 kWh and the maximum charging power is 16 kW. The expected SOC is 0.95. Table 1 shows the random behavior parameters of EVs [22]. The desired voltage range is set from 0.95 to 1.05 p.u. [4]. Figure 6 shows the initial SOC of the EVs. Figure 7 shows the distribution of EV arrival time and departure time. The price is shown in Figure 8.

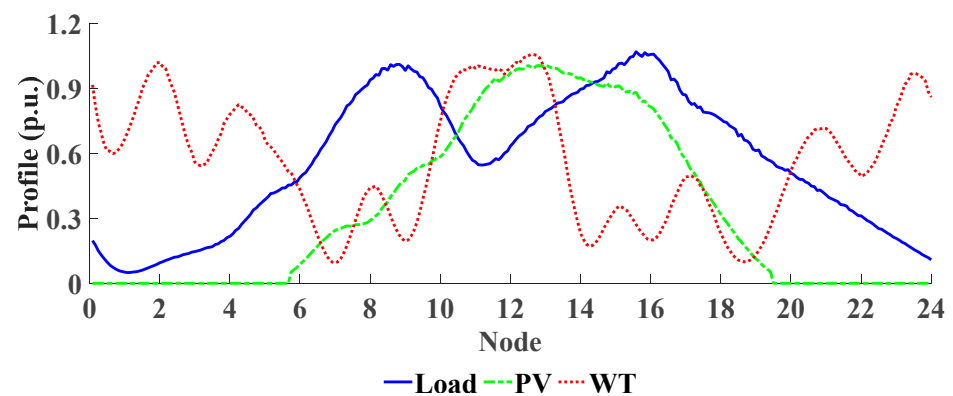


Figure 5. Operational curves of DGs and loads.

Table 1. Random behavior parameters of EVs.

Behaviors	Distribution
Arrival time	N (17.47, 6)
Departure time	N (8.92, 3.25)
Initial SOC	N (0.196, 0.118 ²)

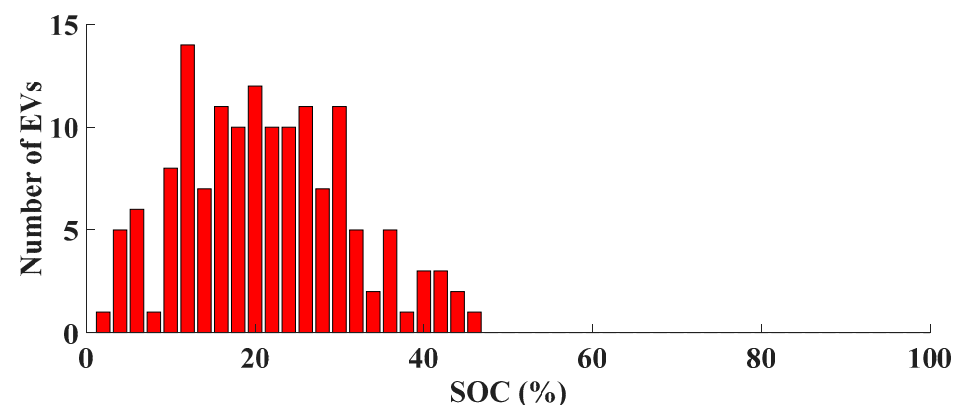


Figure 6. Distribution of initial SOC of EVs.

4.2. Numerical Results

To demonstrate the effectiveness of the proposed method in this paper, three scenarios are adopted as follows.

Scenario I: The initial operational state of FDNs is obtained without strategies of EVs and SOPs.

Scenario II: The proposed data-driven multi-timescale coordination control model is adopted.

Scenario III: The centralized optimization method based on accurate physical parameters is adopted.

Figure 9 illustrates the charging strategies of EVs in three scenarios. Figure 7 shows that EVs mainly arrive at the charging station from 16:00 to 21:00 and depart from the charging station from 5:00 to 10:00. During these periods, EVs in Scenario I are with uncoordinated charging at the charging station. EVs charge at maximum charging power once plugged into the charging station until the SOC reaches expectation. The EVs in Scenario II adopt the charging strategy that is generated by the comprehensive guidance of price and voltage deviation penalty cost. The voltage control effect is shown in Figures 10–13. The charging strategy of EVs in Scenario II is close to that of Scenario III.

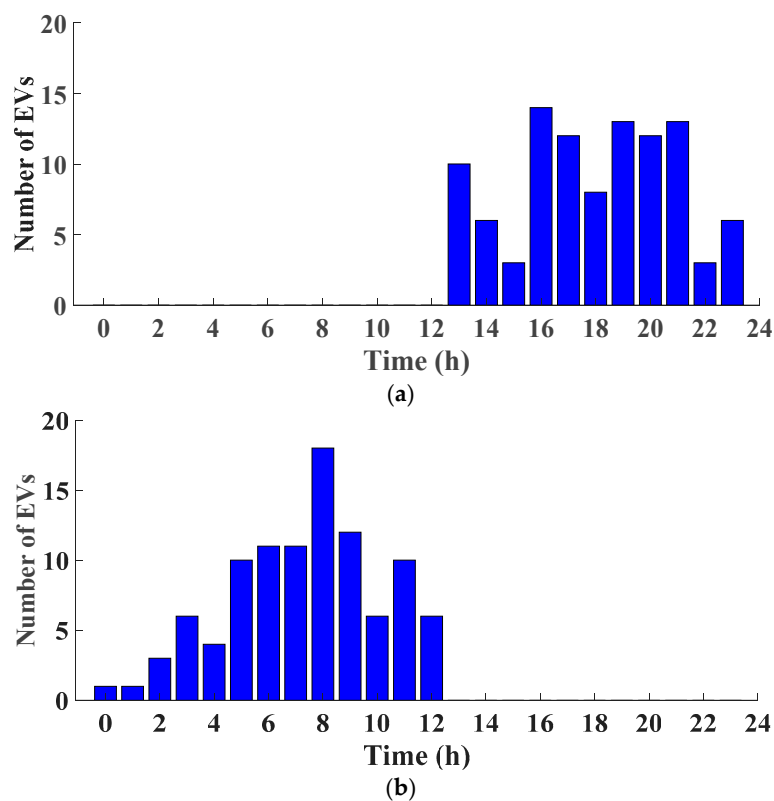


Figure 7. Behavior of EVs. (a) Distribution of EV arrival time; (b) Distribution of EV departure time.

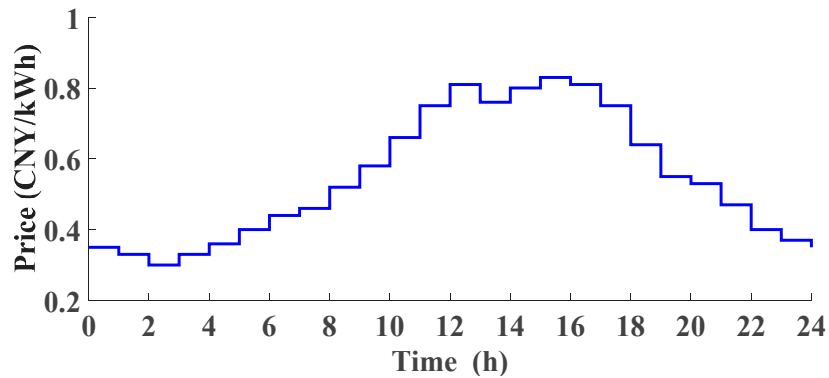


Figure 8. Price of day-ahead market.

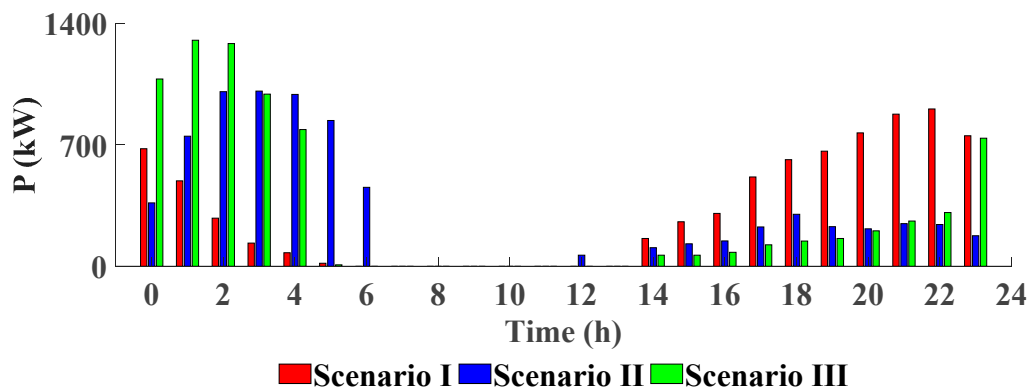


Figure 9. Charging power of each hour in three scenarios.

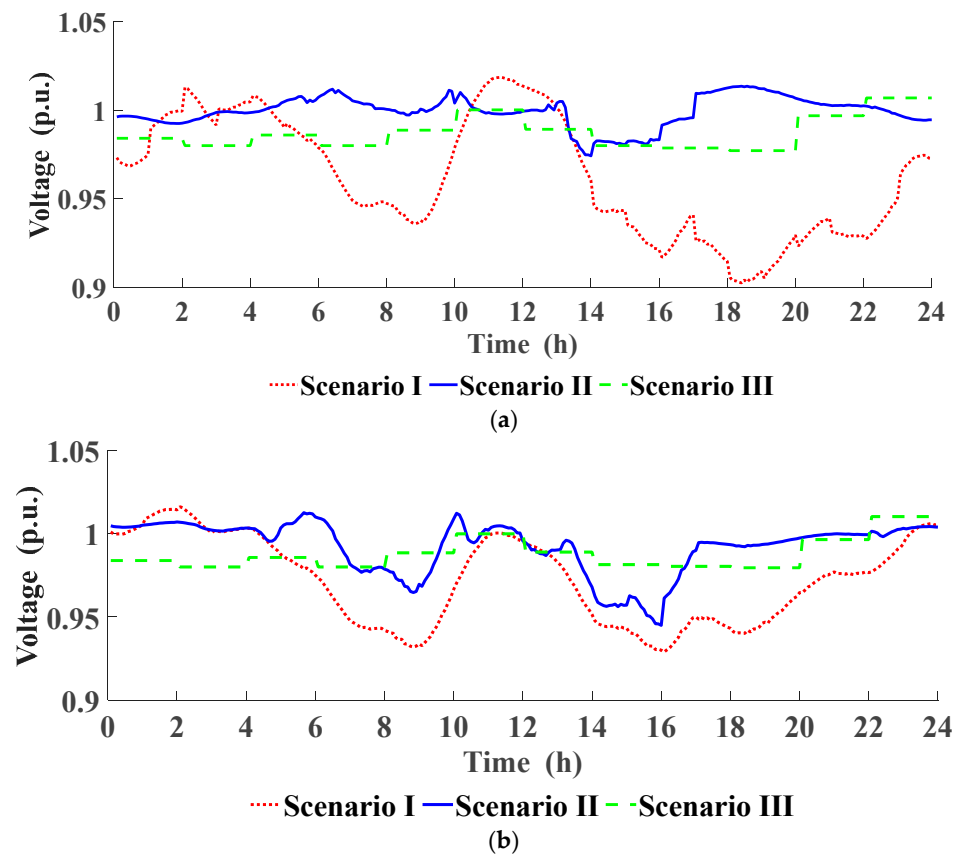


Figure 10. Comparison of voltage profiles. (a) Voltage profiles of Node 18 in three scenarios; (b) Voltage profiles of Node 33 in three scenarios.

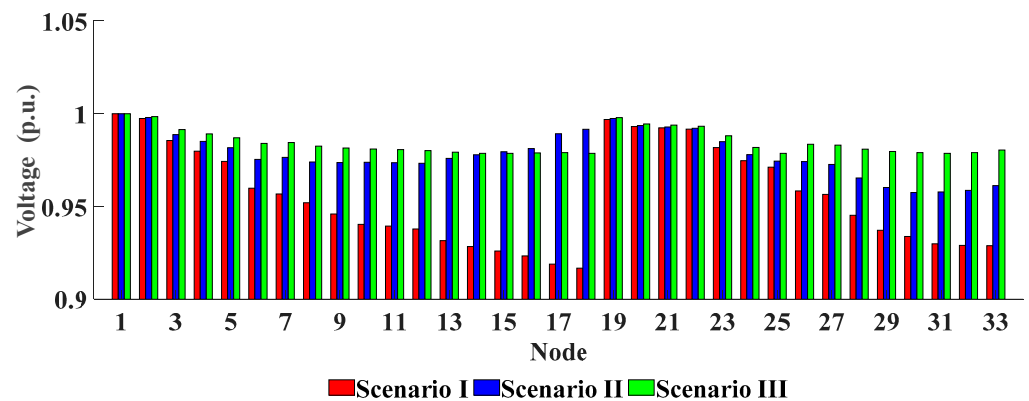


Figure 11. Voltage profiles of all nodes at 16:00.

Figure 10 shows the voltage profiles of Nodes 18 and 33 in three scenarios. Figure 11 shows the voltage profiles of all nodes at 16:00. The maximum and minimum voltages of the whole network at each instant in three scenarios are shown in Figure 12. The uncoordinated charging of EVs and the high penetration of DGs affect the power flow and voltage of FDNs. From 14:00 to 20:00, the uncoordinated charging results in severe voltage deviations. In Scenario II, EVs of type II increase charging power during periods of low price and decrease charging power during periods of high price. The comparison of voltage in Scenarios II and III shows that the voltage control effect of centralized optimization based on accurate physical parameters is slightly better than that of the proposed data-driven method. Moreover, the charging strategy also takes voltage deviations into account. By carrying out the SOP strategy on the fast timescale, the voltage is further maintained within the desired range.

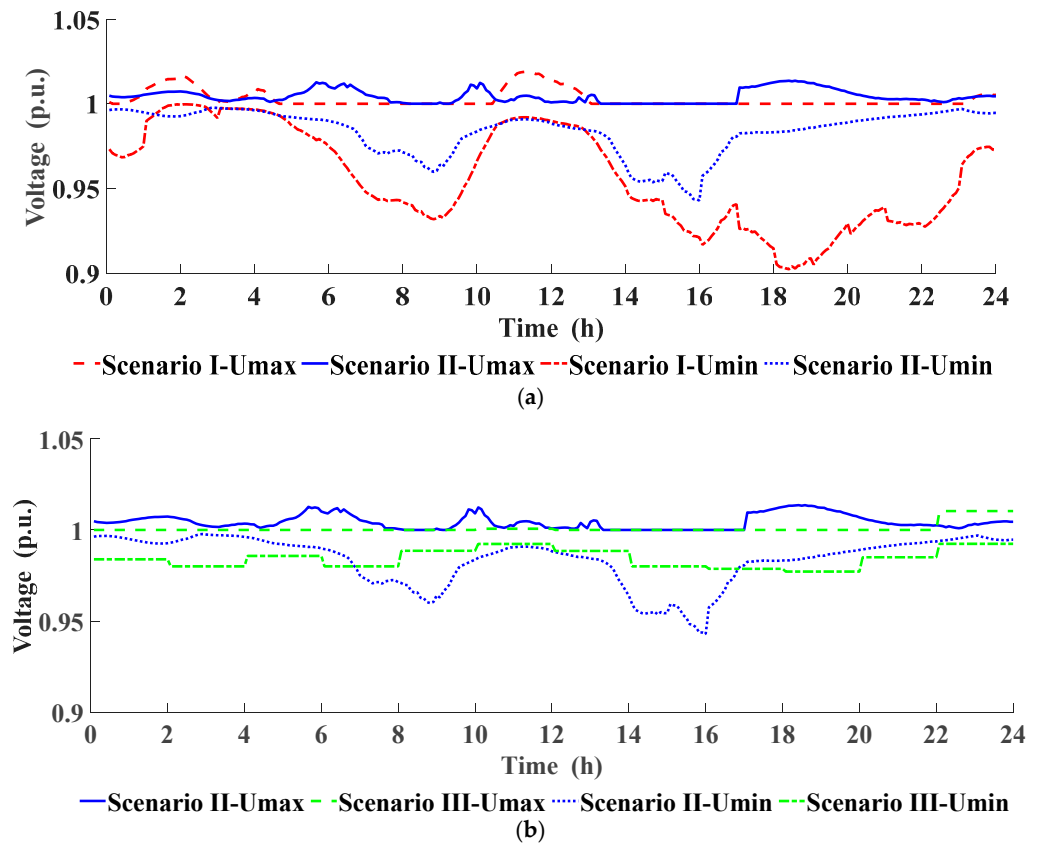


Figure 12. Comparison of maximum and minimum voltages in three scenarios. (a) Maximum and minimum voltages in Scenarios I and II; (b) Maximum and minimum voltages in Scenarios II and III.

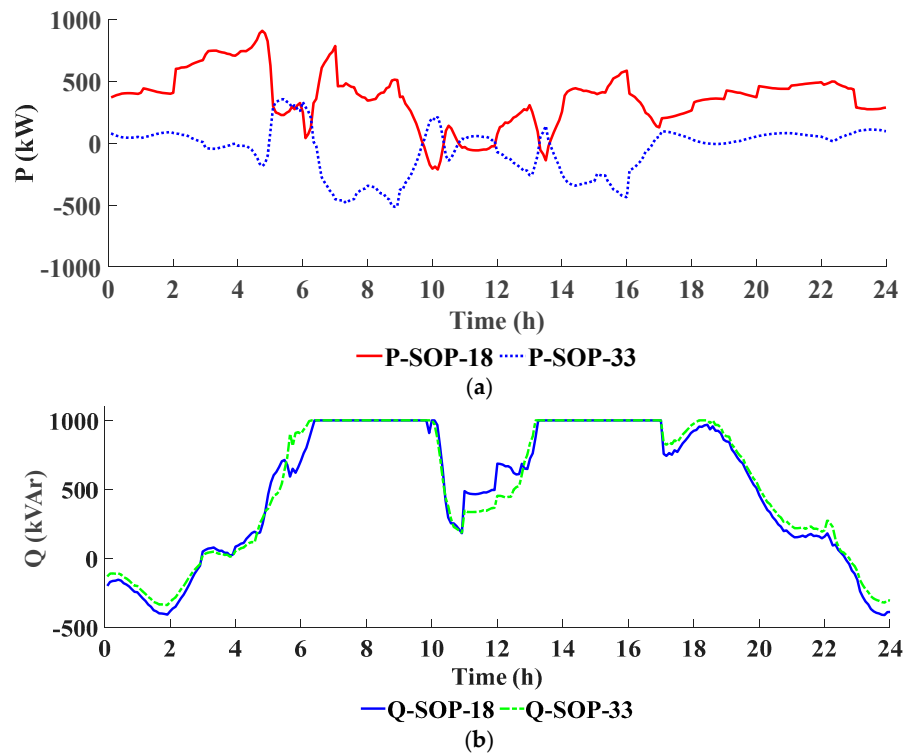


Figure 13. Operation strategy of SOP in Scenario II. (a) Active power transmission of SOP; (b) Reactive power compensation of SOP.

Figure 13 shows the operation strategy of the SOP in Scenario II. It is assumed that extracting power from the grid to the SOP is the positive position. During 18:00–24:00 and 0:00–2:00, the SOP transmits less active power from Node 18 to the charging station due to the low demands of EVs. During 2:00–5:00, the SOP increasingly transmits the active power from Node 18 to the charging station due to the high demands of EVs. During 7:00–9:00 and 14:00–16:00, the active power is transmitted from Node 18 to Node 33 via the SOP, where the power demand of the network is satisfied. Meanwhile, the SOP also regulates the voltage by adjusting the reactive power compensation.

Figure 14 is the comparison of voltage profiles affected by different values of ρ , which shows the parameter sensitivity of the proposed data-driven method. The voltage profiles are essentially similar to each other with $\rho \in [0.8, 1.2]$. The voltage profiles with $\rho \notin [0.8, 1.2]$ may be severely worse than that of Scenario I. The result illustrates that the proposed data-driven method is insensitive to parameters within a predefined range. However, its control performance may be deteriorated when parameters are outside the predefined range.

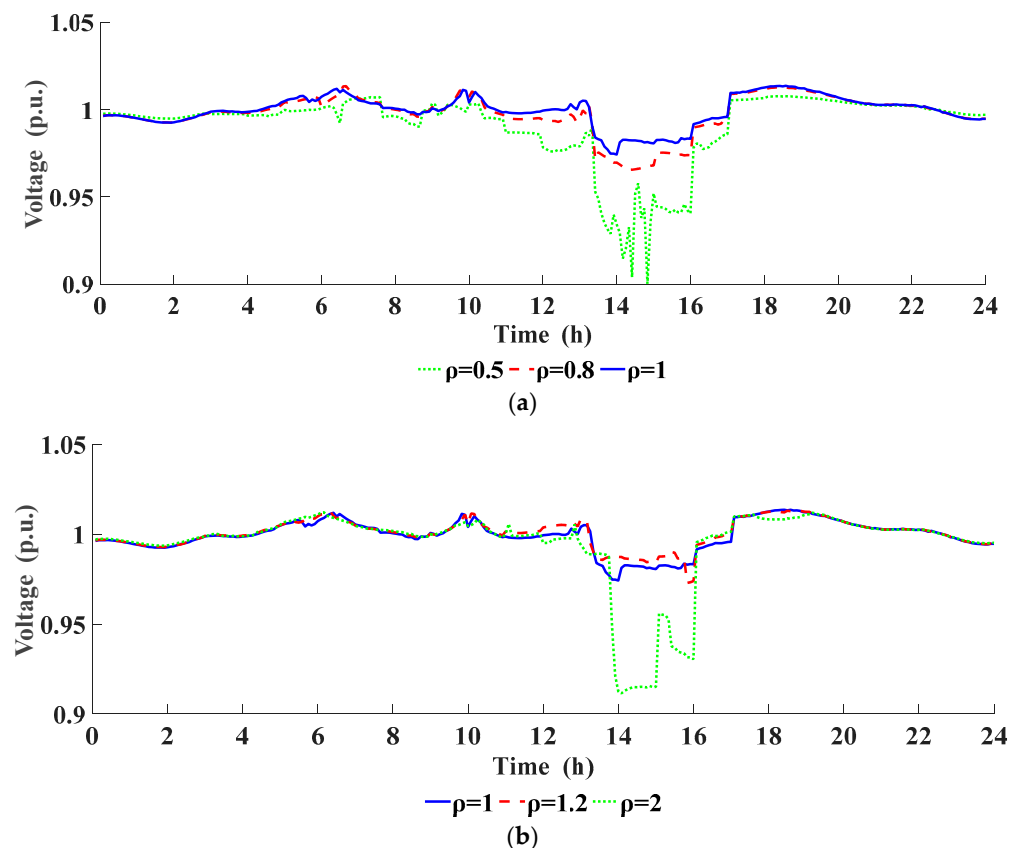


Figure 14. Voltage profiles of Node 18 with different values of ρ . (a) Voltage profiles of Node 18 with $\rho = 0.5, 0.8$ and 1 ; (b) Voltage profiles of Node 18 with $\rho = 1, 1.2$ and 2 .

To quantify the regulation effect of voltage deviations in the above scenarios, the voltage fluctuation index (VFI) is introduced as follows.

$$\text{VFI} = \sum_{i \in \Omega_i} \sum_{t \in T} \left| \mathbf{u}^{\text{ref}} - \mathbf{u}_{i,t} \right| / (N_t N_i) \quad (52)$$

where i denotes the node index. Ω_i denotes the node set of the distribution network. \mathbf{u}^{ref} denotes the voltage reference. $\mathbf{u}_{i,t}$ denotes the voltage of Node i at instant t . N_t denotes the number of control instants in the total control horizon. N_i denotes the number of nodes in distribution networks.

In Table 2, comparing with Scenario I, both the voltage deviation and the electricity purchasing cost in Scenario II are significantly reduced, where the voltage deviation and the

charging cost are reduced by 62.44% and 22%, respectively. The comparison with Scenario III illustrates that the control effect of the proposed method is close to that of centralized optimization based on accurate physical parameters.

Table 2. Comparison of three scenarios.

Scenarios	U _{max} (p.u.)	U _{min} (p.u.)	VFI (p.u.)	Electricity Purchasing Cost (CNY)
I	1.0189	0.9024	0.0205	4078.6
II	1.0136	0.9429	0.0077	3180.1
III	1.0103	0.9770	0.0086	2873.9

In summary, the proposed control model can satisfy the charging demands of EVs. The electricity purchasing cost of charging stations is effectively reduced and the voltage violations of FDNs are alleviated through exploiting the potential of SOP and EVs.

5. Conclusions

This paper proposes a data-driven control framework for FDNs based on the MFAPC without relying on accurate physical parameters. Considering the demands of charging loads and excavating the regulating ability of SOP and EVs, a data-driven multi-timescale coordination control model is established by multi-source data. The proposed model achieves an efficient and flexible operation of FDNs by adjusting the strategy of the SOP and EVs. Moreover, it can also reduce the electricity purchasing cost of charging stations, alleviate voltage deviations, and quickly track the fluctuations of DGs. The case studies and analysis verify the effectiveness and feasibility of the proposed data-driven multi-timescale coordination control method. The proposed framework further provides a promising direction for the control of distribution networks with high penetration of DGs and the large-scale integration of charging loads.

However, data-driven methods heavily rely on data quality, which may have a significant impact on the control effect. Thus, the performance of the proposed method can be further improved through reducing measurement error. Moreover, the interpretability of the proposed data-driven method is necessary to be improved through the integration of model-based methods. Simultaneously, various control devices such as DG converters and on-load tap changers are worthy of consideration. A data-physical hybrid-driven model with multi-device coordination can be further developed to improve the operational performance of FDNs.

Author Contributions: Conceptualization, G.W.; methodology, G.W.; software, Z.Q.; validation, X.F.; formal analysis, W.Z.; investigation, H.R. and J.W.; writing—original draft preparation, G.W.; writing—review and editing, G.W.; visualization, H.J.; supervision, P.L. All authors have read and agreed to the published version of the manuscript.

Funding: This research was funded by [the Science and Technology Project of Guangdong Power Grid Co., Ltd.] grant number [037800KK52200006].

Informed Consent Statement: Not applicable.

Data Availability Statement: Not applicable.

Conflicts of Interest: The authors declare no conflict of interest.

References

- Zhang, Y.; Yang, Y.; Zhang, X.; Pu, W.; Song, H. Planning strategies for distributed pv-storage using a distribution network based on load time sequence characteristics partitioning. *Processes* **2023**, *11*, 540. [\[CrossRef\]](#)
- Maghami, M.R.; Pasupuleti, J.; Ling, C.M. A static and dynamic analysis of photovoltaic penetration into MV distribution network. *Processes* **2023**, *11*, 1172. [\[CrossRef\]](#)
- Xiao, J.; Wang, Y.; Luo, F.; Bai, L.; Gang, F.; Huang, R.; Jiang, X.; Zhang, X. Flexible distribution network: Definition, configuration, operation, and pilot project. *IET Gener. Transm. Distrib.* **2018**, *12*, 4492–4498. [\[CrossRef\]](#)

4. Ji, H.; Wang, C.; Li, P.; Ding, F.; Wu, J. Robust operation of soft open points in active distribution networks with high penetration of photovoltaic integration. *IEEE Trans. Sustain. Energy* **2019**, *10*, 280–289. [[CrossRef](#)]
5. Ding, T.; Wang, Z.; Jia, W.; Chen, B.; Chen, C.; Shahidehpour, M. Multiperiod distribution system restoration with routing repair crews, mobile electric vehicles, and soft-open-point networked microgrids. *IEEE Trans. Smart Grid* **2020**, *11*, 4795–4808. [[CrossRef](#)]
6. Xu, J.; Huang, Y. The short-term optimal resource allocation approach for electric vehicles and V2G service stations. *Appl. Energy* **2022**, *319*, 119200. [[CrossRef](#)]
7. Mehta, R.; Srinivasan, D.; Trivedi, A.; Yang, J. Hybrid planning method based on cost-benefit analysis for smart charging of plug-in electric vehicles in distribution systems. *IEEE Trans. Smart Grid* **2019**, *10*, 523–534. [[CrossRef](#)]
8. Wang, J.; Zhou, N.; Wang, Q.; Liu, H. Hierarchically coordinated optimization of power distribution systems with soft open points and electric vehicles. *Int. J. Electr. Power Energy Syst.* **2023**, *149*, 109040. [[CrossRef](#)]
9. Maulik, A. Probabilistic power management of a grid-connected microgrid considering electric vehicles, demand response, smart transformers, and soft open points. *Sustain. Energy Grids Netw.* **2022**, *30*, 100636.
10. Sun, X.; Qiu, J. A customized voltage control strategy for electric vehicles in distribution networks with reinforcement learning method. *IEEE Trans. Industr. Inform.* **2021**, *17*, 6852–6863. [[CrossRef](#)]
11. Zhu, H.; Zhang, D.; Goh, H.H.; Wang, S.; Ahmad, T.; Mao, D.; Liu, T.; Zhao, H.; Wu, T. Future data center energy-conservation and emission-reduction technologies in the context of smart and low-carbon city construction. *Sustain. Cities Soc.* **2023**, *89*, 104322. [[CrossRef](#)]
12. Tong, L.; Zhao, S.; Jiang, H.; Zhou, J.; Xu, B. Multi-scenario and multi-objective collaborative optimization of distribution network considering electric vehicles and mobile energy storage systems. *IEEE Access* **2021**, *9*, 55690–55697. [[CrossRef](#)]
13. Zhu, X.; Han, H.; Gao, S.; Shi, Q.; Cui, H.; Zu, G. A multi-stage optimization approach for active distribution network scheduling considering coordinated electrical vehicle charging strategy. *IEEE Access* **2018**, *6*, 50117–50130. [[CrossRef](#)]
14. Li, H.; Azzouz, M.A.; Hamad, A.A. Cooperative voltage control in MV distribution networks with electric vehicle charging stations and photovoltaic DGs. *IEEE Syst. J.* **2021**, *15*, 2989–3000. [[CrossRef](#)]
15. Huo, Y.; Li, P.; Ji, H.; Yu, H.; Yan, J.; Wu, J.; Wang, C. Data-driven coordinated voltage control method of distribution networks with high DG penetration. *IEEE Trans. Power Syst.* **2023**, *38*, 1543–1557. [[CrossRef](#)]
16. Lee, Z.J.; Sharma, S.; Johansson, D.; Low, S.H. ACN-Sim: An open-source simulator for data-driven electric vehicle charging research. *IEEE Trans. Smart Grid* **2021**, *12*, 5113–5123. [[CrossRef](#)]
17. Khemmook, P.; Prompinit, K.; Surinkaew, T. Control of a microgrid using robust data-driven-based controllers of distributed electric vehicles. *Electr. Power Syst. Res.* **2022**, *213*, 108681. [[CrossRef](#)]
18. Zhang, X.; Kong, X.; Yan, R.; Liu, Y.; Xia, P.; Sun, X.; Zeng, R.; Li, H. Data-driven cooling, heating and electrical load prediction for building integrated with electric vehicles considering occupant travel behavior. *Energy* **2023**, *264*, 126274. [[CrossRef](#)]
19. Tao, Y.; Qiu, J.; Lai, S. A data-driven management strategy of electric vehicles and thermostatically controlled loads based on modified generative adversarial network. *IEEE Trans. Transp. Electrification* **2022**, *8*, 1430–1444. [[CrossRef](#)]
20. Wang, S.; Li, J.; Hou, Z.; Meng, Q.; Li, M. Composite model-free adaptive predictive control for wind power generation based on full wind speed. *CSEE J. Power Energy Syst.* **2022**, *8*, 1659–1669.
21. Wang, Y.; Hou, Z. Event-triggered model-free adaptive predictive control for nonlinear NCSs with data dropout and application in PMSM control system. In Proceedings of the 2022 IEEE 11th Data Driven Control and Learning Systems Conference (DDCLS), Chengdu, China, 13–15 May 2022; pp. 1111–1117.
22. Zhang, S.; Fang, Y.; Zhang, H.; Cheng, H.; Wang, X. Maximum hosting capacity of photovoltaic generation in SOP-based power distribution network integrated with electric vehicles. *IEEE Trans. Industr. Inform.* **2022**, *18*, 8213–8224. [[CrossRef](#)]

Disclaimer/Publisher’s Note: The statements, opinions and data contained in all publications are solely those of the individual author(s) and contributor(s) and not of MDPI and/or the editor(s). MDPI and/or the editor(s) disclaim responsibility for any injury to people or property resulting from any ideas, methods, instructions or products referred to in the content.